

Supplementary Information

Intelligent and Robust DNA Robots Capable of Swarming into Leakless Nonlinear Amplification in Response to Trigger

Shaofei Li,^{abc} Yizhuang Cheng,^{ac} Miao Qin,^{ac} Guoliang Zhou,^{ac} Pan Li^a and Liangbao Yang^{*ad}

^a Institute of Health and Medical Technology, Hefei Institutes of Physical Science, Chinese Academy of Sciences, Hefei 230031, Anhui, China.

^b School of Life Science, Anhui University, Hefei 230601, Anhui, China.

^c University of Science & Technology of China, Hefei 230026, Anhui, China.

^d Hefei Cancer Hospital, Chinese Academy of Sciences, Hefei 230031, Anhui, China.

* To whom correspondence should be addressed. Email: lbyang@iim.ac.cn

List of Contents

Material and Methods

Supplementary Figures

Dynamical investigation of designed models (Fig. S1-S8).

Thermodynamical investigation of designed models (Fig. S9).

Evaluation of validity of designed models (Fig. S10-S12).

Evaluation of application performance of designed models (Fig. S13-S18).

Supplementary Tables

DNA sequences for investigation of toehold binding (Table S1).

DNA sequences for investigation of smart leak-resistant path controllers as well as multifunctional manipulators. (Table S2).

DNA sequences for investigation of automatic assembly motors (Table S3).

DNA sequences for programming leakless nonlinear amplification (Table S4).

MATERIAL AND METHODS

Oligonucleotides. DNA and miRNA oligonucleotides were synthesized and purified by HPLC (Sangon Biotech Co., China). DNA Hairpins and super-hairpin were prepared as monomers at 5 μM in the reaction buffer (20 mM Tris-HCl, 150 mM KCl, 10 mM $(\text{NH}_4)_2\text{SO}_4$, 5 mM MgCl_2 , 1% Triton X-100, pH 7.5) using a snap cooling procedure: heating at 95°C for 5 min followed by cooling at 0.5°C min^{-1} to 25°C, and allowing equilibration at room temperature for 12 hours before use. The working concentration of DNA Hairpins was 2 μM , and the working concentration of super-hairpins was 0.5~1 μM . The working concentration of the target strands was 10 nM in self-assembly. DNA markers were from were purchased from Sangon Biotech Co., China.

Nanoparticles. Au particles coated with polyvinylpyrrolidone (PVP, MW = 55 000) were prepared according to the previous method.¹ The main process is as follows: Firstly, seed gold was synthesized by trisodium citrate reduction method. Then, seed solution was mixed with sodium citrate solution, hydroxylamine hydrochloride and PVP under vigorous stirring. At last, HAuCl_4 was drop by drop added, and nanoparticles coated with PVP were prepared. The nanoparticles were characterized by scanning electron microscopy images (SIGMA 500).

Exosomes and RNA. Breast cancer cells (MCF-7) were cultured in DMEM medium, supplemented with 10% fetal bovine serum and 100 units ml^{-1} penicillin and 100 $\mu\text{g ml}^{-1}$ streptomycin in an incubator with 5% CO_2 at 37°C. When cells were grown in dishes to 80% confluence, the culture medium supernatant were harvested. The exosomes were isolated from the culture medium by ultracentrifugation.² The isolated exosomes were first examined by transmission electron microscopy (JEM-2100). Then, exosomes were incubated with target strands in PBS for 4 hours at 4°C. After cleaning to remove unbound DNA with PBS, they were further incubated with super-hairpin species in the reaction buffer for 2 hours at room temperature. After cleaning the products with PBS, fluorescence assay was performed using a laser confocal microscope (OLYMPUS FV1000), and also the size distributions of the exosomes were analyzed by dynamic light scattering (Zetasizer Nano ZSP). RNA was extracted from exosomes with TRIzol reagents (Invitrogen).

Gel electrophoresis and ethidium bromide staining. Hybrid products were loaded with 10% glycerol onto 6~8% native polyacrylamide gels prepared with 0.5 \times TBE buffer. Gels were run at 60 V for 45 min at room temperature. Ethidium bromide was used for gel staining and imaged using a gel imaging system (FluorChem E). The relative fluorescence intensity of the hybrid products was estimated by the instrument's own software.

SERS analysis. Label-free SERS applied to detection of the blocked self-assembly products in the gel loading well. Native polyacrylamide gels electrophoresis analysis was performed for self-assembly products without ethidium bromide staining. Nanoparticles were added in the gel loading well ten minutes before the electrophoresis finished. After

nanoparticles were closely arranged, the self-assembly products blocked in the gel loading well were measured on a Lab-RAM HR800 spectrometer with a 633 nm laser. The accumulation time was 5 s with a measured power of 0.9 mW.

AFM imaging. AFM imaging of DNA samples was done on mica sheets (TED PELLA). At first, mica sheet was incubated with 50 μM MgCl_2 solution to increase the strength of the DNA-mica binding for 5 min. Then, mica sheet was washed with ultrapure H_2O for 3~4 times. After drying mica sheet in air, 30 μL of DNA assembly sample was placed on mica sheet for 1 min, followed by washing with ultrapure water for 2 times and drying using a gentle breeze of N_2 .

NUPACK analysis. DNA sequences were analyzed by Nucleic Acids Package (NUPACK) (<http://www.nupack.org/>), which was defined in 1 M Na^+ as a testing benchmark.

Supplementary Figures

Two complementary hairpins (H1-6 and H2-6) with a 6-nt loop and a 6-nt toehold were derived to a series by varying the lengths of toeholds and loops.

In order to reveal the binding dynamics between toeholds and loops, the high CG content was firstly evaluated. Two complementary hairpins of H1-10 and H2-10 were shown with 10 nt toeholds and loops in Fig. S1A, and the details of others derived hairpins were shown in Fig. S1B. As shown in Fig. S1B, CG content in the toehold and loop of each derived hairpin was not less than 50%.

The free energy of each derived hairpin could well meet a testing benchmark of $-16.0 \text{ kcal mol}^{-1}$ which was proposed to resist leakage by the initiation of the reaction in the absence of the initiator.³ There was a slight difference in the overall free energy between derived hairpins where the change was less than $0.5 \text{ kcal mol}^{-1}$ as estimated by NUPACK. The closed-to-open transition requires a sufficiently large amount of energy to unzip the stem.⁴ Therefore, the loop entropy does not play any role in the opening of the hairpin.

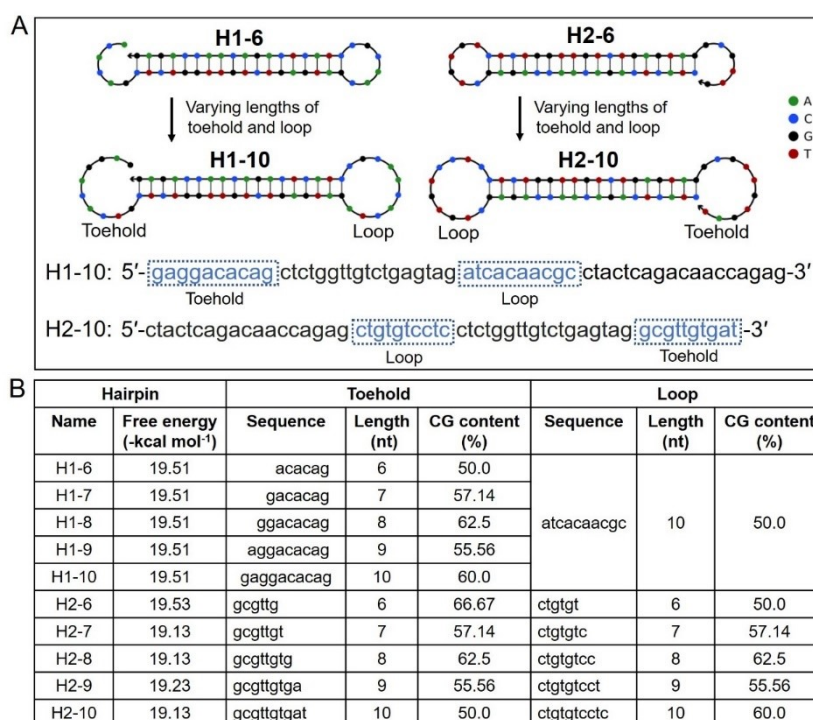


Fig. S1 A derived series from two complementary hairpins by varying lengths of toeholds and loops. CG content was not less than 50% in toehold and loop of each derived hairpin. (A) The derived hairpins. (B) Toeholds, loops and free energies of the derived hairpins.

A single DNA strand is different at its two ends. One end is called 5' (5 prime), and the other is called 3' (3 prime). At each end of the double DNA, one strand is 5' and the other is 3'. The two strands of DNA molecule held together in opposite (anti-parallel) directions by hydrogen bonds. Therefore, the formation of hybrid products should follow these rules. Based on these rules, toeholds and loops between H1 and H2 may match in directions, forming dimers besides the major polymers by reverse complement (Fig. S2A and S2B).

Based on our previous evaluation, DNA hybridization chain reaction can achieve equilibrium within 2 hours in the reaction buffer.³ Here, two pairs of typical hairpins with the different lengths of toeholds and loops were incubated in the reaction buffer for 2 and 24 hours at room temperature. Native polyacrylamide gel electrophoresis was performed to analyze the hybrid products. DNA marker was used as a reference for the relative length of the hybrid products. In fact, DNA hairpins with single- and double-stranded structures and their reaction products are different from complete double-stranded DNA marker.

Similarly, the longer hybrid products appeared only in the mixture of H1-10 and H2-10. Moreover, the relatively short hybrid products, which was about twice the length of a hairpin monomer, also observed only in the mixture of H1-10 and H2-10. Combined with the possibility of dimer formation, we held the opinion that the relatively short hybrid products may be the dimers. Moreover, based on the relative fluorescence intensity, there was no significant change in the results with the extended incubation time (Fig. S2C and S2D).

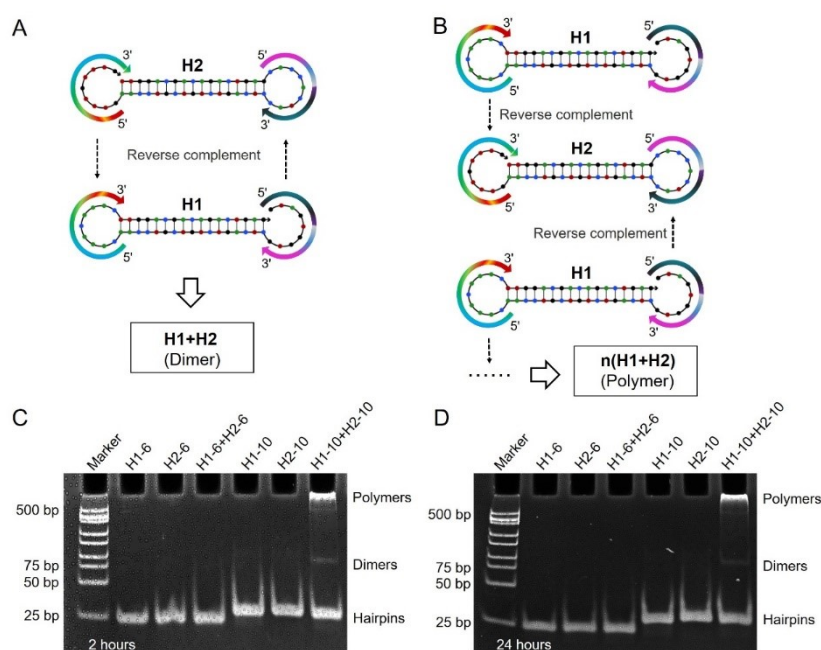


Fig. S2 Native polyacrylamide gel electrophoresis analysis of hybrid products. (A) and (B) Schematic illustration for the binding situations between the derived complementary hairpins. (C) and (D) For 2 and 24 hours in the reaction buffer. Marker is DNA marker A (25~500 bp).

A series were derived from H1-6 and H2-6 by varying sequences and lengths of toeholds and loops with CG content of less than 50% (Fig. S3A and S3B). Each pair of complementary hairpins was incubated in the reaction buffer for 2 hours at room temperature. Similarly, the hybrid products clearly appeared when the lengths of toeholds and loops were extended to 9 nt. Moreover, H1b-69 or H1b-610 with toeholds and loops of 9~10 nt lengths stably coexist with H1b-6 (Fig. S3C), which suggested that the added loop entropy has not caused leakage.

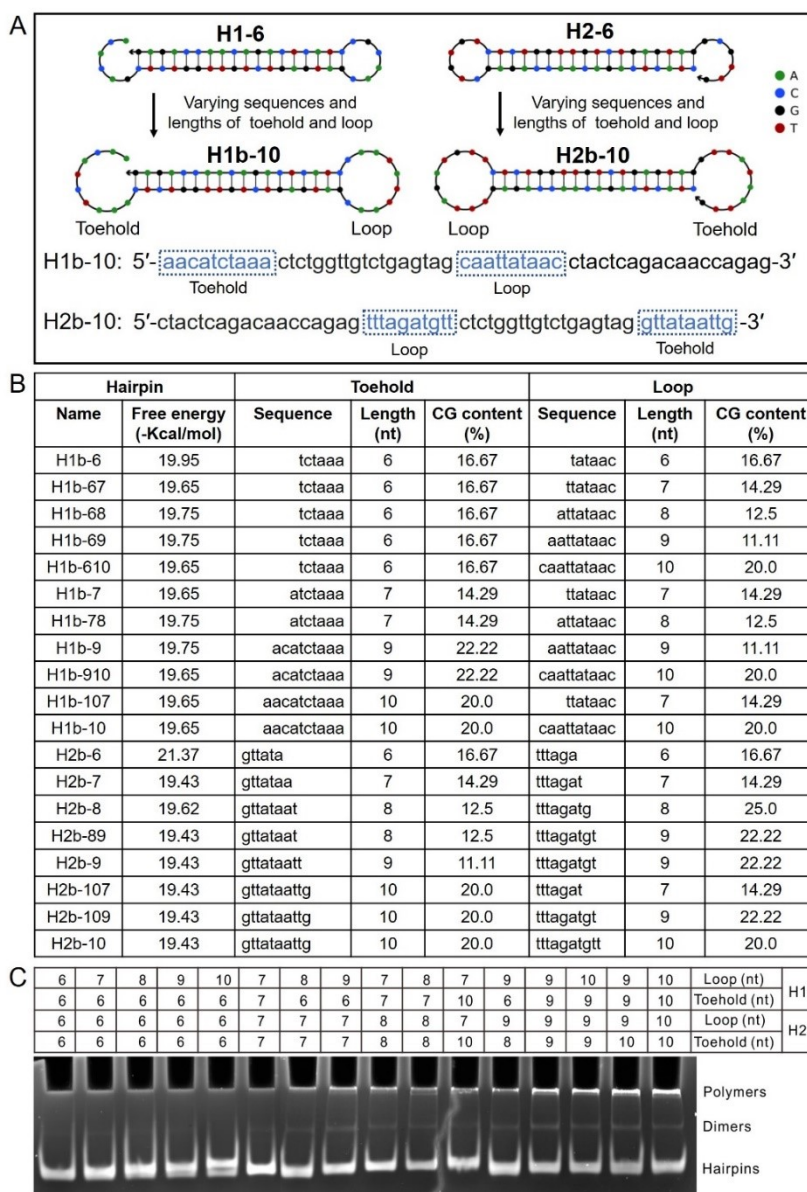


Fig. S3 Binding dynamics between toeholds and loops by varying sequences and lengths. CG contents of toeholds and loops were less than 50%. (A) The derived hairpins. (B) Toeholds, loops and free energies of the derived hairpins. (C) Native polyacrylamide gel electrophoresis analysis for hybrid products.

A series were derived from H1-6 and H2-6 by varying sequences of stems, as well as lengths of toeholds and loops (Fig. S4A and S4B). Especially, A-T base pairs were used in stem next to the toehold, and some shorter toeholds were also evaluated. The free energy of each derived hairpin could meet a testing benchmark of $-16.0 \text{ kcal mol}^{-1}$. Each pair of complementary hairpins was incubated in the reaction buffer for 2 hours at room temperature. Similarly, the hybrid products clearly appeared when the lengths of toehold and loop were extended to 9 nt (Fig. S4C). Moreover, good stability was maintained between complementary hairpins with short toeholds of less than 7 nt and long loops of 9~10 nt, which suggested that the added loop entropy has not caused leakage.

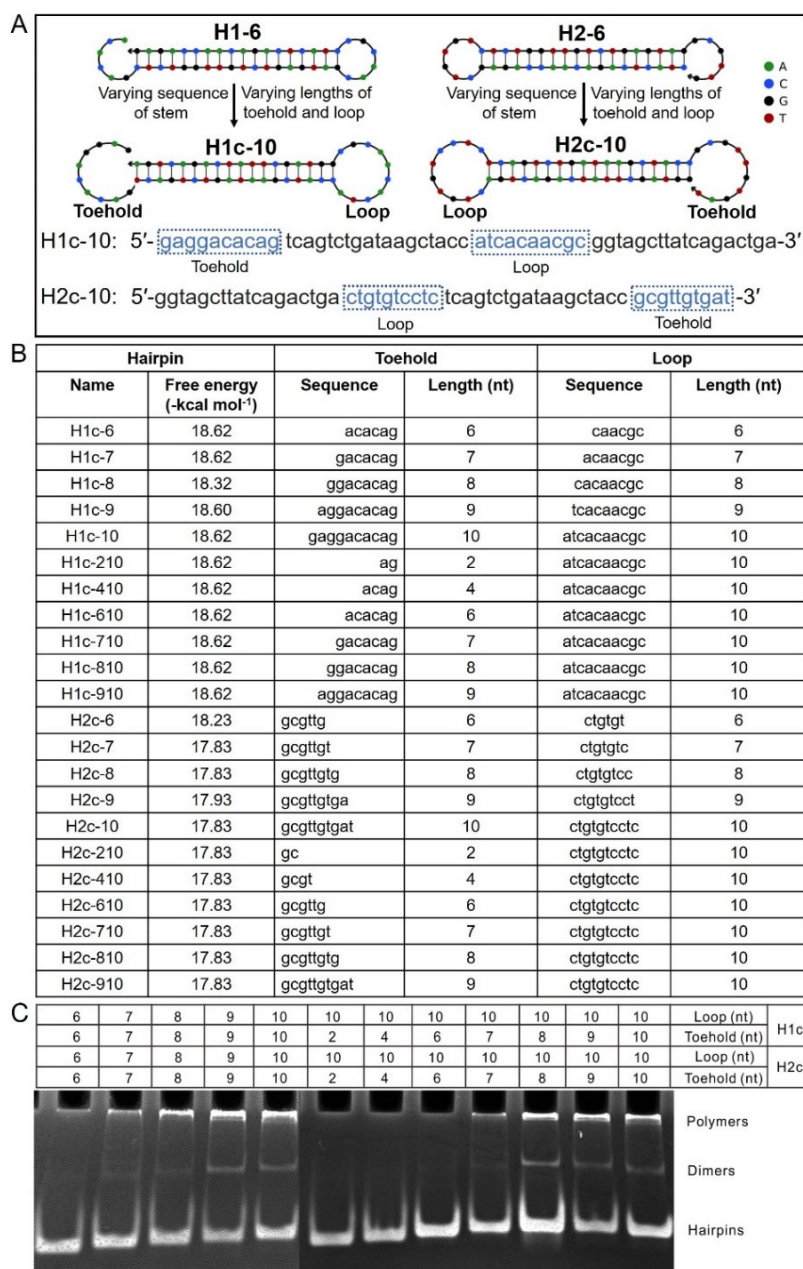


Fig. S4 Toehold binding dynamics between toeholds and loops by varying the sequences of stems. (A) The derived hairpins. (B) Toeholds, loops and free energies of the derived hairpins. (C) Native polyacrylamide gel electrophoresis analysis for hybrid products.

Eight pairs of complementary hairpins with toeholds and loops of 9 nt lengths were randomly selected. The free energy of each hairpin could meet a testing benchmark of $-16.0 \text{ kcal mol}^{-1}$. The sequences of hairpins were detailed in Table S1. Each pair of complementary hairpins was incubated in the reaction buffer for 2 hours at room temperature. Similarly, both dimers and polymers appeared (Fig. S5). The results indicated that toehold and loop of 9 nt lengths can be used as a general parameter for binding between toeholds and loops.

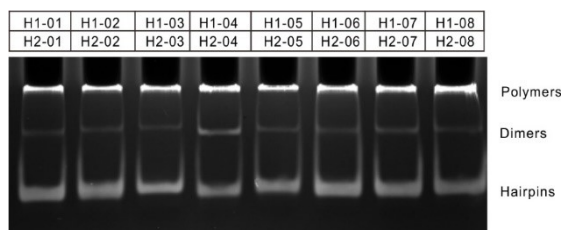


Fig. S5 Toehold binding dynamics between toeholds and loops by using some random complementary hairpins. Eight pairs of complementary hairpins with toeholds and loops of 9 nt lengths were randomly selected. Native polyacrylamide gel electrophoresis analysis showed the hybrid products.

Several pairs of typical hairpins in Fig. S3-5 were also compared in the reaction buffer for 2 and 24 hours at room temperature. Native polyacrylamide gel electrophoresis was performed to analyze the hybrid products. Similarly, no significant differences were found in the hybrid products at different incubation times (Fig. S6).

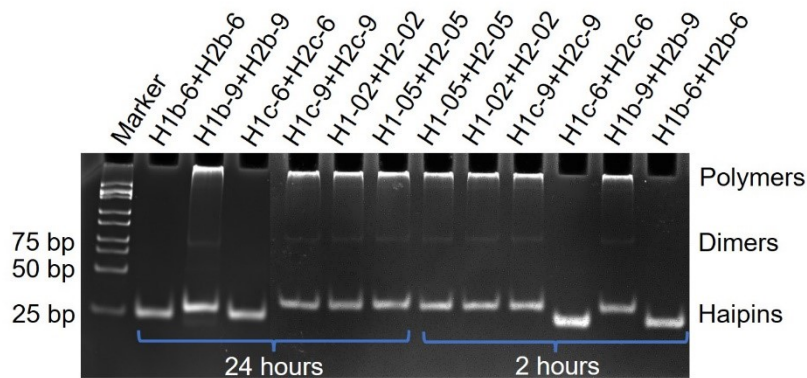


Fig. S6 Native polyacrylamide gel electrophoresis analysis of hybrid products. Marker is DNA marker A (25–500 bp).

According to our previous research, transient melting of DNA hairpin stem can occur to cause of leakage and that can be mitigated through consideration of the sequence thermodynamics³. If the stem of hairpins could be opened spontaneously, two complementary hairpins maybe hybridize in turn to form a long leakage product (Fig. S7). To prevent that from happening, the free energy of DNA hairpins could meet a testing benchmark of $-16.0 \text{ kcal mol}^{-1}$ to resist leakage.³

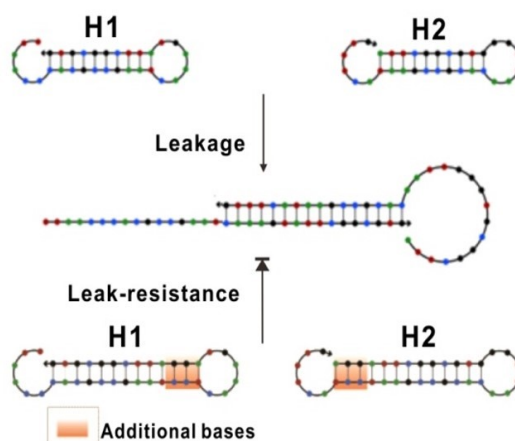


Fig. S7 Schematic illustration of leakage hybridization and leak-resistance. Leakage hybridization can form the long products between complementary hairpins and that can be mitigated through consideration of the sequence thermodynamics.

As mentioned above (Fig. S2), the two strands of DNA molecule held together in opposite directions by hydrogen bonds. Unlike the traditional hairpins (Fig. S2A and S8A), toeholds and loops between V_1 and V_2 may not match in directions to form dimers (Fig. S8B). On the contrary, they should form the long polymers by alternate combination one by one (Fig. S8C).

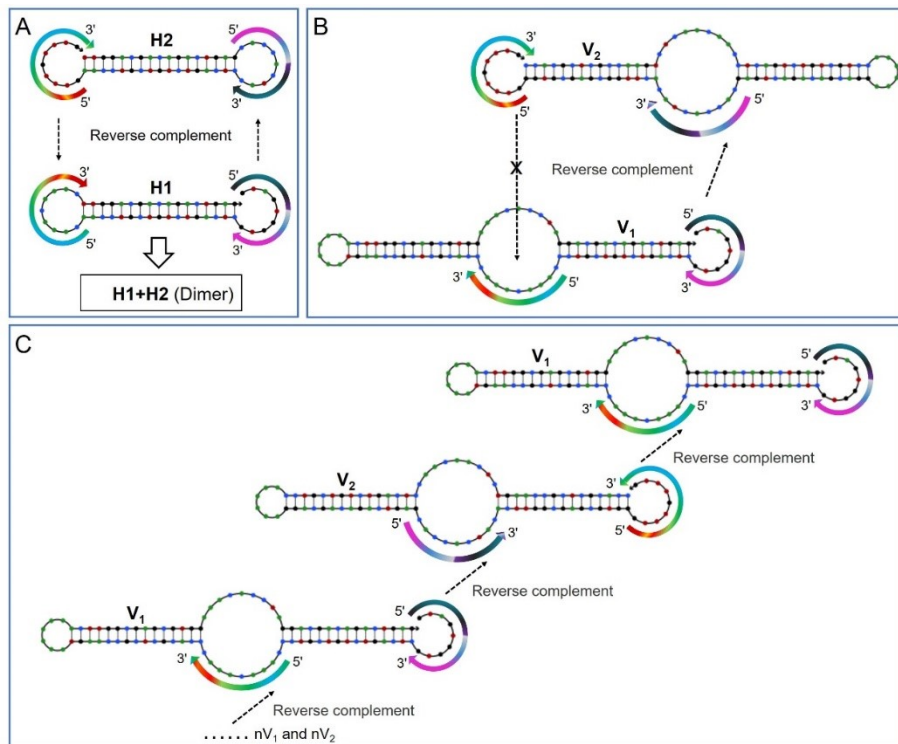


Fig. S8 Schematic illustration for the binding situations between the derived complementary hairpins. (A) H1 and H2. (B) and (C) V_1 and V_2 .

A series of super-hairpins were derived from W_1 and R_2 by varying the lengths of one multifunctional manipulator of each super-hairpin species (Table S3 and Fig. S9A). The probability of a resting microstate were estimated by NUPACK (Fig. S9B).

The sequestered bases of 3 nt lengths were the same in W_{1a} and W_{2a-2} . Therefore two identical stem domains of four-branch migration could exchange equally along a complementary regions. As shown in Fig. S9B, four-branch migration could be carried out to expose the next sequestered bases although W_{1a} and W_{2a-2} have only one multifunctional manipulator each. On the contrary, the sequestered bases of 3 nt lengths were different in others complementary super-hairpins. Four-branch migration could only be carried out to expose the next sequestered bases when the length of the varied manipulator was not less than 6 nt.

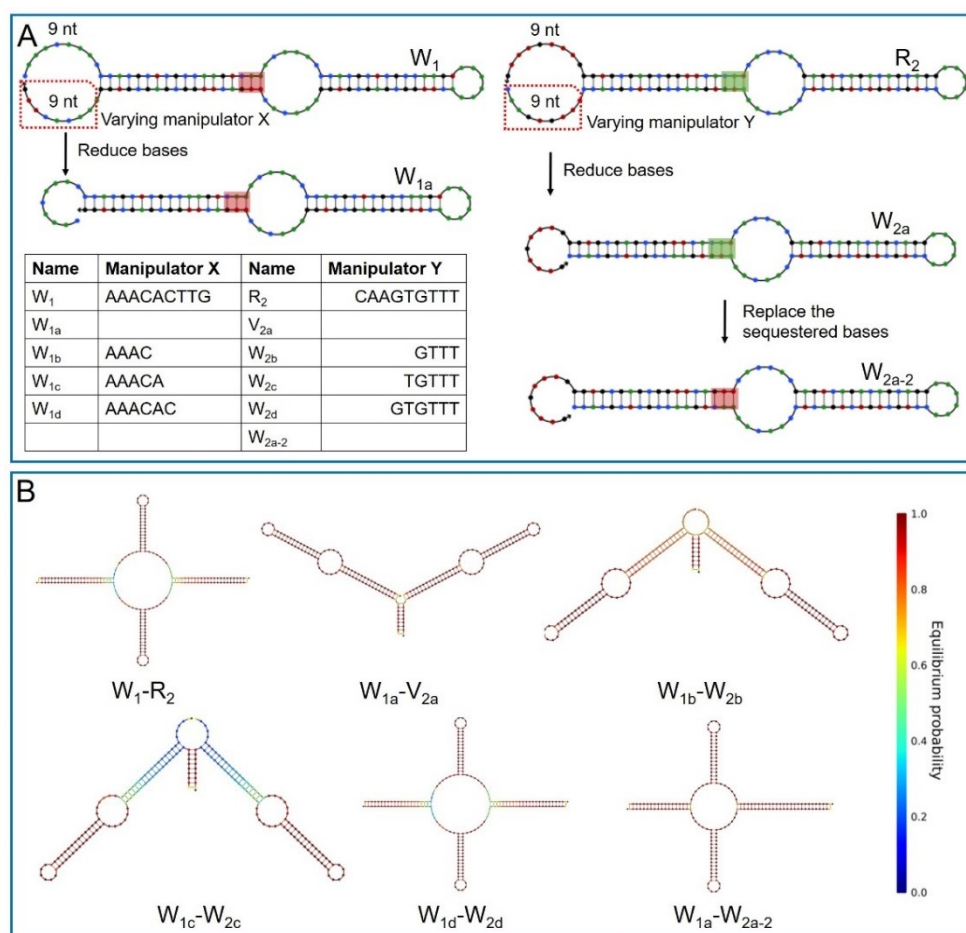


Fig. S9 The probability of a resting microstate estimated for the forming complex between the derived hairpins. (A) The derived hairpins. (B) The depicted state of the derived hairpins at equilibrium.

Minimum free energy (MFE) structures were estimated by NUPACK. The sequestered bases, with lengths of 3 nt, were different between the two two intelligent DNA robots (Table S4 and Fig. S10A). Moreover, the free energy of each stem domain met a testing benchmark of $-16.0 \text{ kcal mol}^{-1}$ to resist leakage. After the combination of T and R_1 , the first smart leak-resistant path controller was opened, which provided the docking locations for two manipulators of R_2 (Fig. S10B). And then, two automatic assembly motors could run along with four-branch migration so that two leak-resistant path controllers were further opened (Fig. S10C).

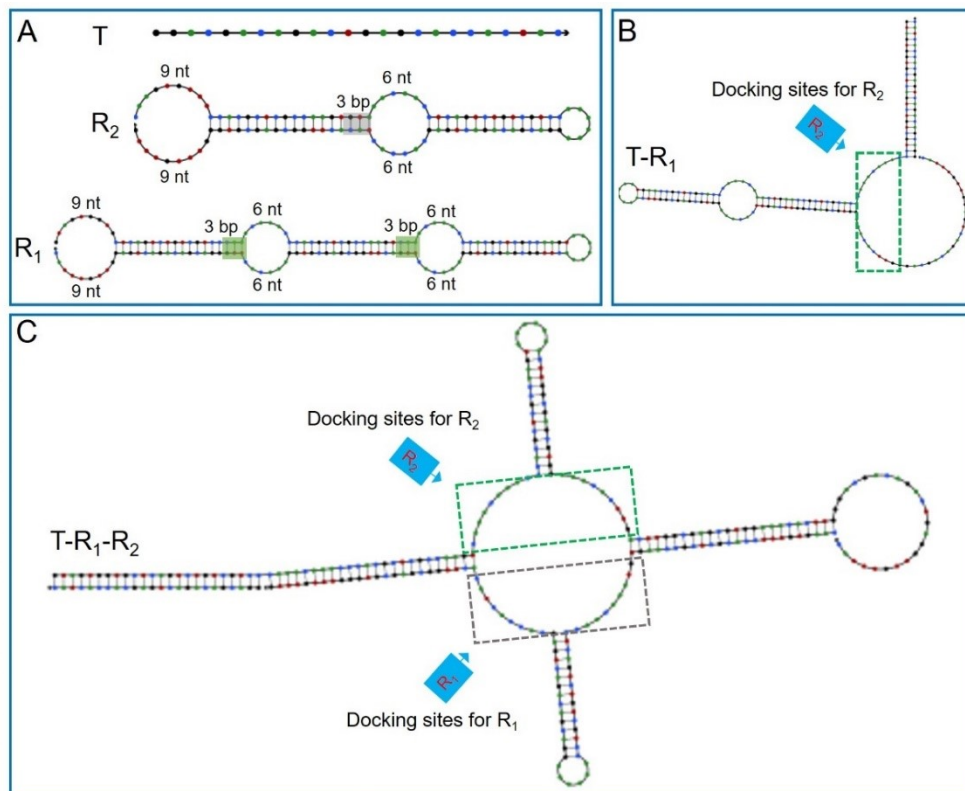


Fig. S10 MFE structures estimated by NUPACK. (A) T, R_1 and R_2 . (B) Complex of T- R_1 . (C) Complex of T- R_1 - R_2 .

R₁, R₂ and T were incubated in the reaction buffer for different times at room temperature. Native polyacrylamide gel electrophoresis analysis showed the reaction products. As shown in Fig. S11A, no significant differences were found in the assembly products after 2 hours.

Moreover, two traditional hairpins (H_{t1} and H_{t2}) were also designed to target T in linear hybridization chain reaction (Table S4). According to the analysis of 4% native polyacrylamide gel electrophoresis analysis, linear products in hybridization chain reaction were widely distributed in size and nonlinear ones were relatively distributed in long fragments.

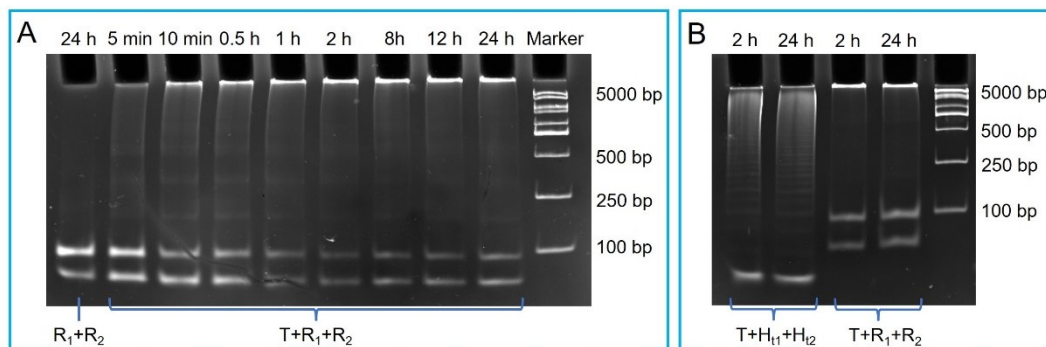


Fig. S11 4% Native polyacrylamide gel electrophoresis analysis for nonlinear amplification. (A) At different incubation times. (B) Comparison of linear and nonlinear amplification products.

The running steps for nonlinear amplification were also explored by native polyacrylamide gel electrophoresis analysis. DNA marker was used as a reference for the relative length of the hybrid products. In the initial step, excess T could completely consume R1 to form complexes T-R1, and vice versa (Fig. S12A-a1 and S12B-b1). Next, excess T and R₂ could completely consume R1 to form complexes T-R₁-R₂ and T-R₁-2R₂, and excess R₂ could completely consume T-R₁ to form long polymers step by step (Fig. S12A-a2 and S12B-b2). Moreover, the formation process of polymers could be optimized by decreasing the concentration of T and increasing the concentration of R2 (Fig. S12A-a3 and S12B-b3). These results supported the designed assembly pathway.

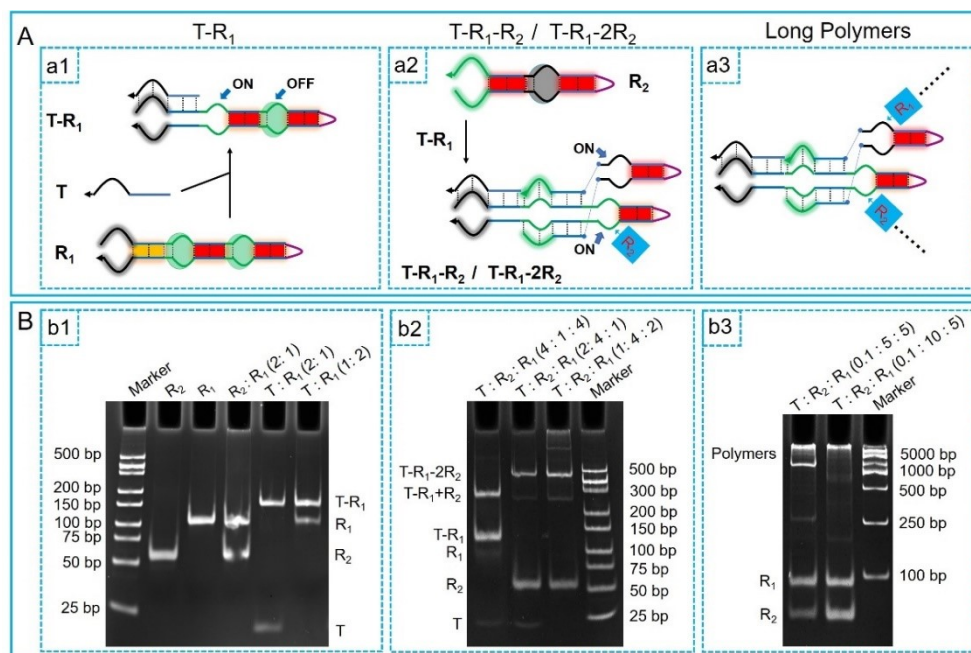


Fig. S12 Evaluation of assembly products on the running steps. (A) Schematic illustrations for assembly products on the running steps. (B) Native polyacrylamide gel electrophoresis analysis.

Atomic force microscopy (AFM) imaging was done on mica sheets. Compared with the morphology in the absence of trigger, the tiny yellow spots were assembled in dendrimers in the presence of trigger (Fig. S13A and S13B).

Moreover, because DNA self-assembly was carried out in a high-salt solution, the thorough washing was not performed in order to preserve the original morphology of assembly products. Therefore, some salts were remained on mica sheets, which may show irregular white spots.

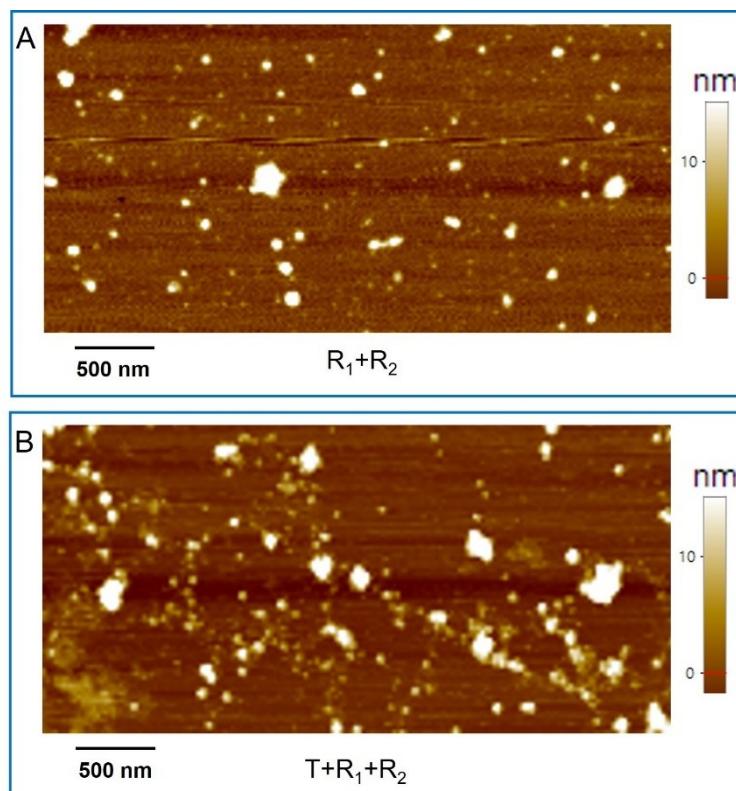


Fig. S13 Atomic force microscopy images. (A) The presence and (B) the absence of trigger T1. DNA shows yellow spots, and some salts show irregular white spots.

Minimum free energy (MFE) structures were estimated by NUPACK. The sequestered bases, with lengths of 3 nt, were different between the two two intelligent DNA robots (Table S4 and Fig. S14A). Moreover, the free energy of each stem domain met a testing benchmark of $-16.0 \text{ kcal mol}^{-1}$ to resist leakage. After the combination of T_b and R_{1b} , the first smart leak-resistant path controller was opened, which provided the docking locations for two manipulators of R_{2b} (Fig. S14B). And then, two automatic assembly motors could run along with four-branch migration so that two leak-resistant path controllers were further opened (Fig. S14C).

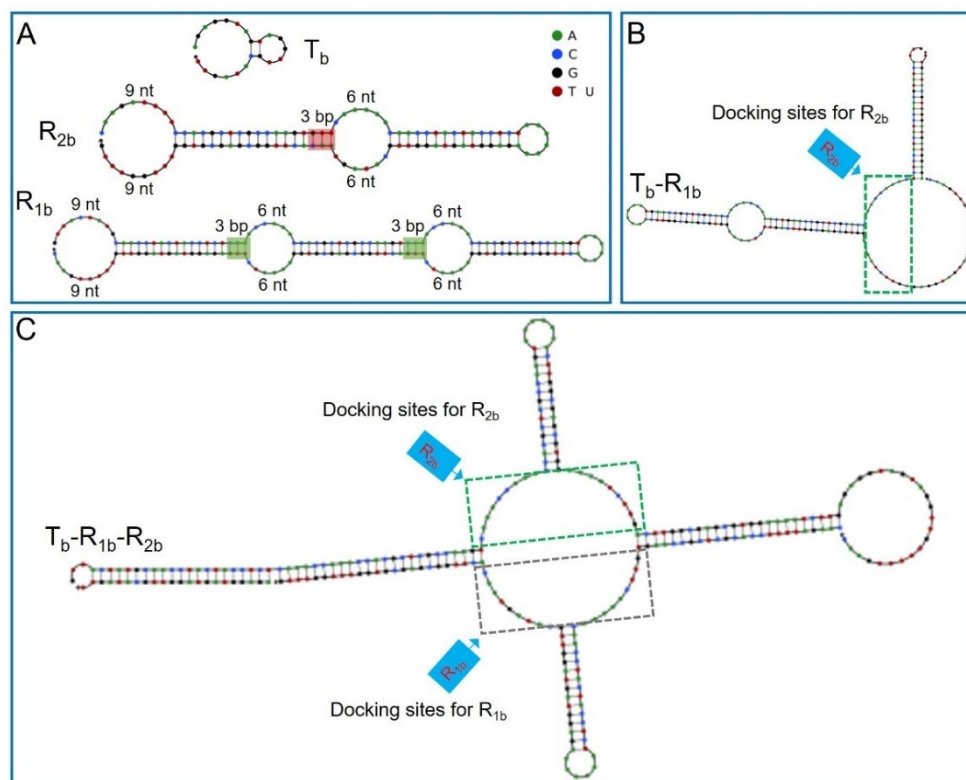


Fig. S14 MFE structures estimated by NUPACK. (A) T_b , R_{1b} and R_{2b} . (B) Complex of T_b - R_{1b} . (C) Complex of T_b - R_{1b} - R_{2b} .

Minimum free energy (MFE) structures were estimated by NUPACK. The sequestered bases, with lengths of 3 nt, were different between the two two intelligent DNA robots (Table S4 and Fig. S15A). Moreover, the free energy of each stem domain met a testing benchmark of $-16.0 \text{ kcal mol}^{-1}$ to resist leakage. After the combination of T_c and R_{1c} , the first smart leak-resistant path controller was opened, which provided the docking locations for two manipulators of R_{2c} (Fig. S15B). And then, two automatic assembly motors could run along with four-branch migration so that two leak-resistant path controllers were further opened (Fig. S15C).

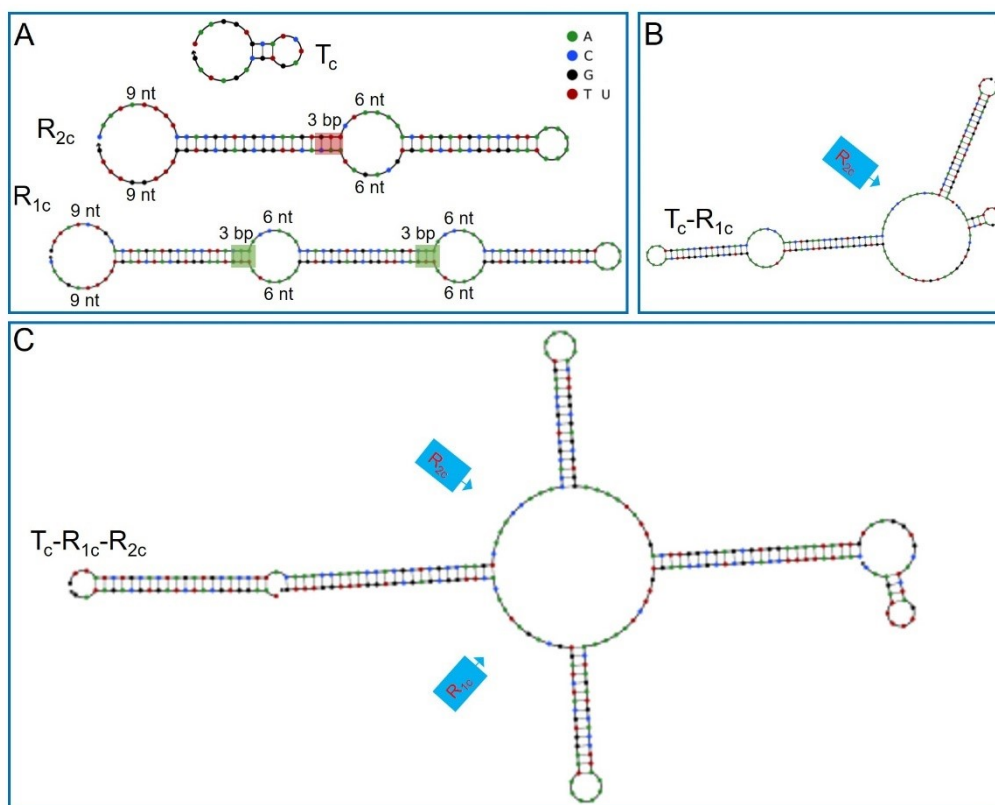


Fig. S15 MFE structures estimated by NUPACK. (A) T_c , R_{1c} and R_{2c} . (B) Complex of T_c-R_{1c} . (C) Complex of $T_c-R_{1c}-R_{2c}$.

SERS is a commonly used sensing technique with several attractive properties, such as high speed, small amount of sample, comparatively low cost and so on.⁵

Label-free SERS was fulfilled as follow. 4% Native polyacrylamide gels electrophoresis without ethidium bromide staining was firstly performed to isolate the assembly products. And then nanoparticles were added in the gel loading well. After nanoparticles were closely arranged, the long assembly products blocked in the gel loading wells were measured by direct SERS readout (Fig. S16).

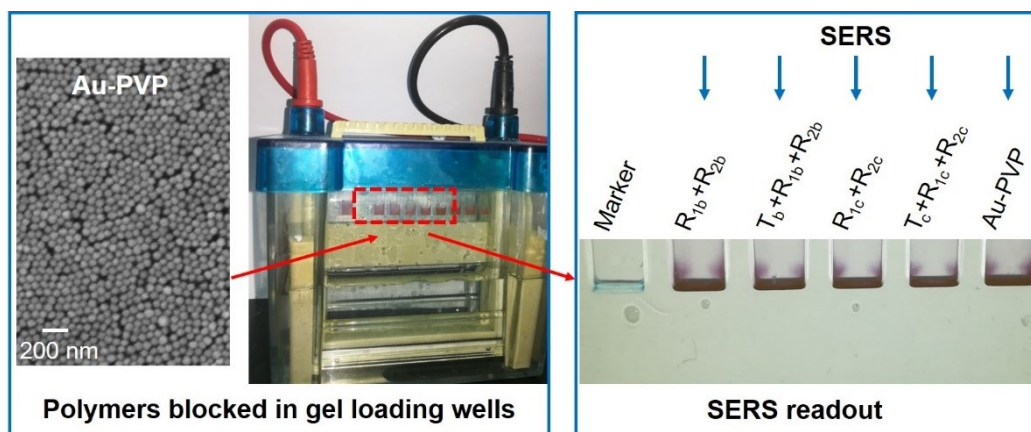


Fig. S16 Label-free SERS readout for assembly products blocked in the gel loading wells.

DNA aptamers are short single-stranded nucleic acids that can bind to specific targets with high affinity and play critical roles in molecular recognition.⁶ They are screened from in vitro synthesized random single stranded DNA libraries. Aptamers can also be coupled to other molecular to trigger a downstream function.^{7, 8}

CD63 is a commonly found membrane bound protein in exosomes.⁹ The sequence of CD63 aptamer was designed according to relevant reference.¹⁰ CD63 aptamer was fused in 5'-terminal of target T.

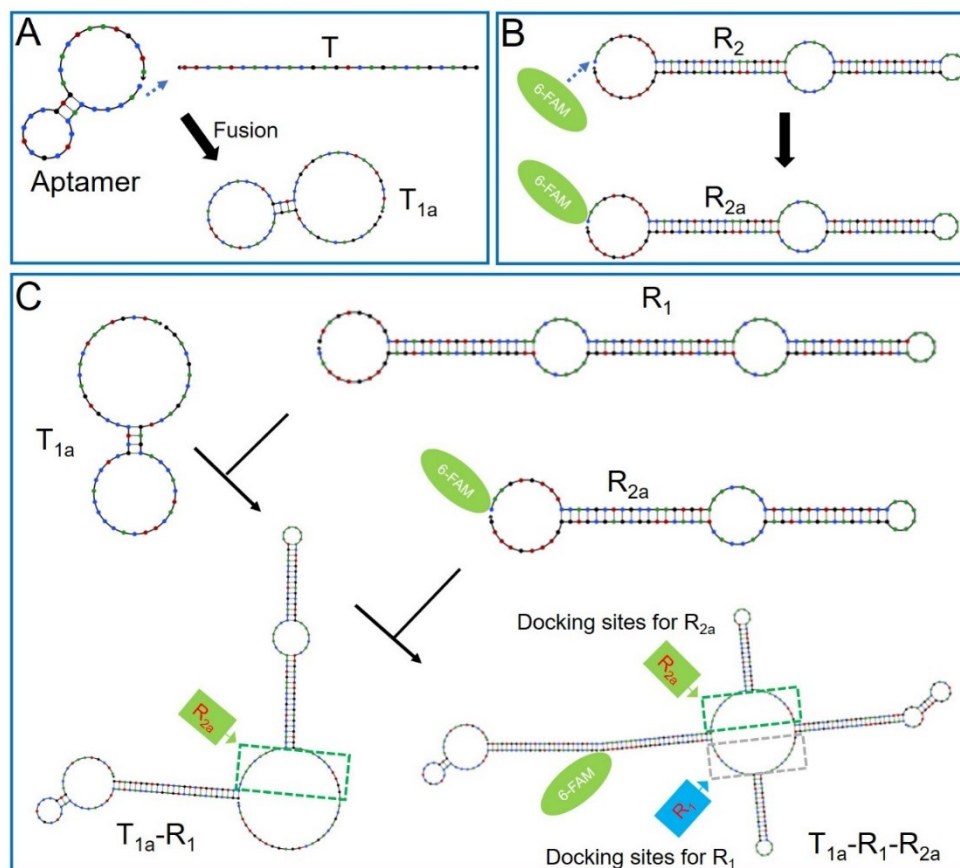


Fig. S17 MFE structures estimated by NUPACK. (A) T_{1a} . CD63 aptamer was fused in 5'-terminal of T_{1a} . (B) R_{2a} . 5'-terminal of R_{2a} was modified by the fluorescent dye (6-FAM). (C) The primary assembly complexes.

Exosomes are 30-150 nm in size and contain miRNAs.¹¹ The loss and overexpression of miRNAs are involved in diseases, which may serve as potential biomarkers.¹²

Has-let-7d-5p (Tb) has proved that was involved in the development and progression of breast cancer.¹³ RNA was extracted from exosomes of breast cancer cells (MCF-7) (Fig. S18A). The extracted RNA was amplified separately in linear and nonlinear reaction systems (Table S4). Similar to using Tb as trigger, the amplification products were observed in two systems. According to the analysis of 4% native polyacrylamide gel electrophoresis analysis, linear products were widely distributed in size and nonlinear ones were relatively distributed in long fragments (Fig. S18B). To further evaluate potential amplification capability, Tb with different concentrations were evaluated in nonlinear reaction system by the provided label-free SERS (Fig. S16), and the limit of detection (LOD) for Tb was about 0.004 nM (Fig. S18B). Similarly, the extracted RNA with different concentrations were evaluated (Fig. S18C). Thus, the diluted concentration of Has-let-7d-5p in RNA can be evaluated by comparing it to LOD. Correspondingly, native polyacrylamide gel electrophoresis analysis was performed. Label-free SERS, by contrast, showed better sensitivity.

Of course, we also observed that the transitional bands emerged into the gel (Fig. S18E). By optimizing the gel concentration, it may be possible to further improve the potential of the limit of detection.

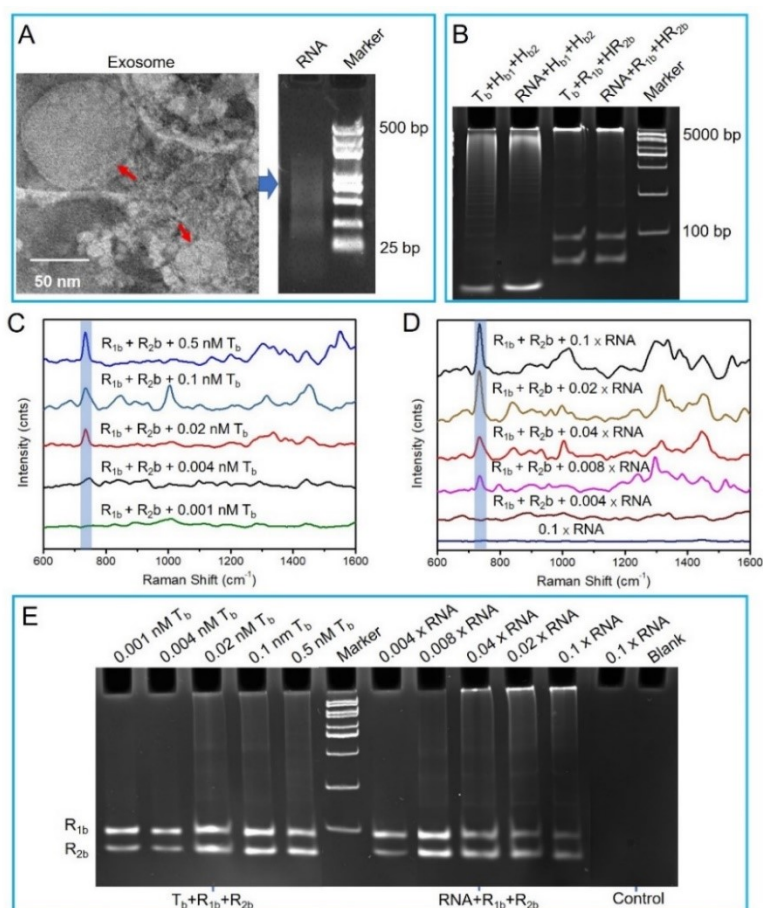


Fig. S18 Evaluation of the application performance of designed models. (A) Exosomes and RNA characterized by transmission electron microscopy and native polyacrylamide gel electrophoresis. The red arrows indicate exosomes. (B) and (E) 4% Native polyacrylamide gel electrophoresis analysis for assembly products. (C) and (D) Label-free SERS analysis for assembly products. The blue band indicates the marker of DNA at $\sim 732\text{ cm}^{-1}$.

Name	Strand sequences (5' to 3')	Free energy (-kcal mol ⁻¹)
H1-01	TGTTTGGGTCCGATCAGACTGCATCATCACAAACGGATGCAGTCTGATCGG	18.74
H2-01	GATGCAGTCTGATCGGACCCAAACAACCGATCAGACTGCATCCGTTGTGAT	18.57
H1-02	CTTAACCTCAGATCCTAAGCCGCACATCAGCAAACATATGTGCGGCTTAGGATCT	21.02
H2-02	ATGTGCGGCTTAGGATCTGAGGTTAAGAGATCCTAAGCCGCACATAGTTTGCTG	20.98
H1-03	CACTTAACCTCAGATCCTAAGCCGCTCCACAAAGTAGCGGCTTAGGATCTGA	19.66
H2-03	AGCGGCTTAGGATCTGAGGTTAAGTGCAGATCCTAAGCCGCTACTTTGTGG	20.13
H1-04	GCACTAGATGCACCTAGACTACACTCCTAGGTGCATCTAGTGCACCTGTGAG	19.23
H2-04	GAGTGTAGTCTAGGTGCATCTAGTGCCTCACAAGTGCAGTGCAGTGCACCTAG	18.99
H1-05	GCAGTGCCTGATGAACGCTCCTTCATCGTTCATCACGCACTGCACCTATGGAA	21.92
H2-05	ATGAAGGAGCGTTCATCACGCACTGCTCCATAGTGCAGTGCCTGATGAACG	22.02
H1-06	CACGCCGAATCCTAGAACCCAAACATCTAGGATTCGGCGTGCGTTGTGGT	18.70
H2-06	TGTTTGGGTCTAGGATTCGGCGTGACCCACAACGCACGCCGAATCCTAGA	18.77
H1-07	CACGCCGAATCTGGTGCGCAGCCACCACCAGATTCGGCGTGTTCCTTCG	19.99
H2-07	GTGGCTGCGCACCAGATTCGGCGTGCGAAGGAACCACGCCGAATCTGGTG	20.27
H1-08	GTAGTGGTGCTCAGTCTGTCGTCCAAACAACAACTTGGACGACAGACTGAG	19.34
H2-08	TTGGACGACAGACTGAGCACCACTACCTCAGTCTGTCGTCCAAAGTTTGTGG	18.98

Table S1. DNA sequences for investigation of toehold binding.

The blue bases constitute the exposed toeholds, and the red ones constitute the loops.

Table S2. DNA sequences for investigation of smart leak-resistant path controllers as well as multifunctional manipulators.

Name	Strand sequences (5' to 3')
V _{1a}	GTAGTGGTGCTCAGTCTGTCGTCCCAAACAACCCACGCTCGCCAAGTAAAAAACTTGGCGAGCGT GGAAACACTTGGGACGACAGACTGAG
V _{2a}	CCACGCTCGCCAAGTGTAACAACCTCAGTCTGTCGTCCAAAAAAGGACGACAGACTGAGCACCCT ACACTTGGCGAGCGTGGGTTTGTGTTG
V ₁	GTAGTGGTGCTCAGTCTGTCGTCCCAAACAACCCACGCTCGCCAAGTAAAAAACTTGGCGAGCGT GGAAACACTTAGGACGACAGACTGAG
V ₂	CCACGCTCGCCAAGTCTCAACAACCTCAGTCTGTCGTCCAAAAAAGGACGACAGACTGAGCACCCT ACACTTGGCGAGCGTGGGTTTGTGTTG

Table S3. DNA sequences for investigation of automatic assembly motors.

Name	Strand sequences (5' to 3')
W ₁	CAAACAAACCCACGCTCGCCAAGTCAAACAAACCCACGCTCGCCAAGTAAAAAACTTGGCGAGCG TGGAACACTTGACTTGGCGAGCGTGGAACACTTG
R ₂	CAAGTGTTCCACGCTCGCCAAGTGTAAACAACCTCAGTCTGTCGTCCAAAAAGGACGACAGACTG AGCACCCTACACTTGGCGAGCGTGGGTTTGTGTTG
W _{1a}	CAAACAAACCCACGCTCGCCAAGTCAAACAAACCCACGCTCGCCAAGTAAAAAACTTGGCGAGCG TGGAACACTTGACTTGGCGAGCGTGG
W _{1b}	CAAACAAACCCACGCTCGCCAAGTCAAACAAACCCACGCTCGCCAAGTAAAAAACTTGGCGAGCG TGGAACACTTGACTTGGCGAGCGTGGAAC
W _{2b}	GTTTCCACGCTCGCCAAGTGTAAACAACCTCAGTCTGTCGTCCAAAAAGGACGACAGACTGAGCAC CACTACACTTGGCGAGCGTGGGTTTGTGTTG
W _{1c}	CAAACAAACCCACGCTCGCCAAGTCAAACAAACCCACGCTCGCCAAGTAAAAAACTTGGCGAGCG TGGAACACTTGACTTGGCGAGCGTGGAACA
W _{2c}	TGTTTCCACGCTCGCCAAGTGTAAACAACCTCAGTCTGTCGTCCAAAAAGGACGACAGACTGAGCA CCACTACACTTGGCGAGCGTGGGTTTGTGTTG
W _{1d}	CAAACAAACCCACGCTCGCCAAGTCAAACAAACCCACGCTCGCCAAGTAAAAAACTTGGCGAGCG TGGAACACTTGACTTGGCGAGCGTGGAACAC
W _{2d}	GTGTTTCCACGCTCGCCAAGTGTAAACAACCTCAGTCTGTCGTCCAAAAAGGACGACAGACTGAGC ACCACTACACTTGGCGAGCGTGGGTTTGTGTTG
W _{2a-2}	CCACGCTCGCCAAGTCAAACAACCTCAGTCTGTCGTCCAAAAAGGACGACAGACTGAGCACCAC TTGACTTGGCGAGCGTGGGTTTGTGTTG

Table S4. DNA sequences for investigation of leakless nonlinear amplification

Name	Strand sequences (5' to 3')
T	GGACGACAGACTGAGCACCCTACTAC
R ₁	GTAGTGGTGCTCAGTCTGTCGTCCCAACAAACCCACGCTCGCCAAGTCAAACAAACCCA CGCTCGCCAAGTAAAAAACTTGGCGAGCGTGGAAACACTTGACTTGGCGAGCGTGGAA ACACTTGGGACGACAGACTGAGGTTGTTTAC
R ₂	CAAGTGTTTCCACGCTCGCCAAGTGTAACAACCTCAGTCTGTCGTCCAAAAAAGGACGA CAGACTGAGCACCCTACTACTTGGCGAGCGTGGGTTTGTGTTG
H ₁₁	GTGGTGCTCAGTCTGTCGTCCCAACAGGACGACAGACTGAG
H ₁₂	GGACGACAGACTGAGCACCCTCAGTCTGTCGTCCCTGTTTG
T _b (Has-let-7d-5p)	AGAGGUAGUAGGUUGCAUAGUU
R _{1b}	GTTACTATGCAACCTACTACCTCTCAAACCAAACCCACGCTCGCCAAGTCAAACCAAACCCAC GCTCGCCAAGTAAAAAACTTGGCGAGCGTGGAAAATCTTGACTTGGCGAGCGTGGAAAA TCTTG AGAGGTAGTAGGTTGTTTTGAAC
R _{2b}	CAAGATTTTCCACGCTCGCCAAGTGTTCAAAAACAACCTACTACTCTAAAAAAGAGGTA GTAGGTTGCATAGTAACACTTGGCGAGCGTGGTGTGTTTG
H _{b1}	AACTATGCAACCTACTACCTCTCAA ACCAGAGGTAGTAGGTTGC
H _{b2}	AGAGGTAGTAGGTTGCATAGTTGCAACCTACTACTCTGGTTTG
T _c (Hsa-miR-18a-5p)	UAAGGUGCAUCUAGUGCAGAUAG
R _{1c}	GTTATCTGCACTAGATGCACCTTACAAACCAAACCCACGCTCGCCAAGTCAAACCAAACCA CGCTCGCCAAGTAAAAAACTTGGCGAGCGTGGAAAATATTGACTTGGCGAGCGTGG AAAA TATTGTAAGGTGCATCTAGTTTTTGAAC
R _{2c}	CAATATTTTCCACGCTCGCCAAGTGTTCTAAAACTAGATGCACCTTAAAAAATAAGGTG CATCTAGTGCAGATAAC ACTTGGCGAGCGTGGTGTGTTTG
T _{1a}	GGACGACAGACTGAGCACCCTACTTCACCCCACCTCGCTCCCGTGACACTAATGCTA
R _{2a}	6-FAM/CAAGTGTTTCCACGCTCGCCAAGTGTAACAACCTCAGTCTGTCGTCCAAAAAG GACGACAGACTGAGCACCCTACTACTTGGCGAGCGTGGGTTTGTGTTG

REFERENCES

1. B. Zhou, M. Mao, X. Cao, M. Ge, X. Tang, S. Li, D. Lin, L. Yang and J. Liu, *Anal Chem*, 2018, **90**, 3826-3832.
2. F. Marqués-García and M. Isidoro-García, in *Molecular Genetics of Asthma*, 2016, DOI: 10.1007/978-1-4939-3652-6_11, ch. Chapter 11, pp. 153-167.
3. S. Li, P. Li, M. Ge, H. Wang, Y. Cheng, G. Li, Q. Huang, H. He, C. Cao, D. Lin and L. Yang, *Nucleic Acids Res*, 2020, **48**, 2220-2231.
4. K. Oertell, E. M. Harcourt, M. G. Mohsen, J. Petruska, E. T. Kool and M. F. Goodman, *PNAS*, 2016, **113**, E2277-E2285.
5. A. I. Pérez-Jiménez, D. Lyu, Z. Lu, G. Liu and B. Ren, *Chem Sci*, 2020, **11**, 4563-4577.
6. X. Fu, F. Peng, J. Lee, Q. Yang, F. Zhang, M. Xiong, G. Kong, H. M. Meng, G. Ke and X. B. Zhang, *Top Curr Chem (Cham)*, 2020, **378**, 21.
7. B. D. Wilson, A. A. Hariri, I. A. P. Thompson, M. Eisenstein and H. T. Soh, *Nat Commun*, 2019, **10**.
8. J. D. Munzar, A. Ng and D. Juncker, *Nat Commun*, 2018, **9**, 343.
9. S. A. Melo, L. B. Luecke, C. Kahlert, A. F. Fernandez, S. T. Gammon, J. Kaye, V. S. LeBleu, E. A. Mittendorf, J. Weitz, N. Rahbari, C. Reissfelder, C. Pilarsky, M. F. Fraga, D. Piwnica-Worms and R. Kalluri, *Nature*, 2015, **523**, 177-182.
10. Y. Xia, M. Liu, L. Wang, A. Yan, W. He, M. Chen, J. Lan, J. Xu, L. Guan and J. Chen, *Biosens Bioelectron*, 2017, **92**, 8-15.
11. S. Aday, I. Hazan-Halevy, A. Chamorro-Jorganes, M. Anwar, M. Goldsmith, N. Beazley-Long, S. Sahoo, N. Dogra, W. Sweaad, F. Catapano, S. Ozaki-Tan, G. D. Angelini, P. Madeddu, A. V. Benest, D. Peer and C. Emanuelli, *Mol Ther*, 2021, **29**, 2239-2252.
12. A. P. Ferragut Cardoso, M. Banerjee, A. N. Nail, A. Lykoudi and J. C. States, *Semin Cancer Biol*, 2021, **76**, 120-131.
13. N. Zhang, H. Zhang, Y. Liu, P. Su, J. Zhang, X. Wang, M. Sun, B. Chen, W. Zhao, L. Wang, H. Wang, M. S. Moran, B. G. Haffty and Q. Yang, *Cell Death Differ*, 2019, **26**, 843-859.